

Thermalization in Quantum Fluids of Light: A Convection-Diffusion Equation

Vladislav Yu. Shishkov,* Ivan V. Panyukov, and Evgeny S. Andrianov

*Dukhov Research Institute of Automatics (VNIIA),
22 Sushchevskaya, Moscow 127055, Russia; and*

Moscow Institute of Physics and Technology, 9 Institutskiy pereulok, Dolgoprudny 141700, Moscow region, Russia;

Anton V. Zasedatelev†

*Vienna Center for Quantum Science and Technology (VCQ), Faculty of Physics,
University of Vienna, Boltzmanngasse 5, 1090 Vienna, Austria*

(Dated: January 22, 2025)

We develop a microscopic theory for the dynamics of quantum fluids of light, deriving an effective kinetic equation in momentum space that takes the form of the convection-diffusion equation. In the particular case of two-dimensional systems with parabolic dispersion, it reduces to the Bateman–Burgers equation. The hydrodynamic analogy unifies nonlinear wave phenomena, such as shock wave formation and turbulence, with non-equilibrium Bose–Einstein condensation of photons and polaritons in optical cavities. We introduce the Reynolds number (Re) and demonstrate that the condensation threshold corresponds exactly to a critical Reynolds number of unity ($Re = 1$), beyond which ($Re > 1$) a shock-like front emerges in the momentum space, characterized by the Bose–Einstein distribution for the particle density in states with high momentum.

I. INTRODUCTION

Quantum fluids of light exhibit remarkable collective behaviors driven by nonlinear interactions between photons or polaritons, giving rise to a diverse array of hydrodynamical phenomena [1]. Thermalization of the particles is a crucial process in the formation of light-matter Bose–Einstein condensates (BECs) [2–4]. In optical cavities, this process depends on the absorption and emission of photons by dye molecules within the cavity. In this case, the rate of energy exchange between the cavity photons and the molecules, as well as their vibrational properties, significantly impacts the efficiency of thermalization. In this study, we develop an effective equation that describes the kinetics of particles over momentum space, resembling the Bateman–Burgers equation [5, 6] known from fluid dynamics. We introduce the concept of the Reynolds number (Re) for the two-dimensional Bose gas and show that the critical value of this number ($Re = 1$) not only marks the onset of significant nonlinear dynamics, but also coincides with the threshold for Bose–Einstein condensation.

II. KINETICS OF THE BOSE GAS

The dynamics of the average number of particles, $n_{\mathbf{k}}(t)$, with momentum \mathbf{k} is governed by three processes: thermalization, dissipation with the rate $\gamma_{\mathbf{k}}$, and incoherent pumping with the rate $\varkappa_{\mathbf{k}}(t)$ which may depend on time. Generally, the kinetics of the Bose gas can be

described by the Maxwell–Boltzmann equation [7].

$$\frac{\partial n_{\mathbf{k}}(t)}{\partial t} = -\gamma_{\mathbf{k}} n_{\mathbf{k}}(t) + \sum_{\mathbf{k}'} \left[\gamma_{\text{therm}}^{\mathbf{k}\mathbf{k}'} (n_{\mathbf{k}}(t) + 1) n_{\mathbf{k}'}(t) - \gamma_{\text{therm}}^{\mathbf{k}'\mathbf{k}} (n_{\mathbf{k}'}(t) + 1) n_{\mathbf{k}}(t) \right] + \varkappa_{\mathbf{k}}(t), \quad (1)$$

An important property of the particles affecting their kinetics is their dispersion, $\omega_{\mathbf{k}}$, that establishes the connection between the momentum of the particle, $\hbar\mathbf{k}$, and its energy, $\hbar\omega_{\mathbf{k}}$. We assume that (1) the system is isotropic, that is, the energy of the particles and the dissipation rate depend only on the absolute value of the momentum, k , i.e. $\hbar\omega_{\mathbf{k}} = \hbar\omega_k$ and $\gamma_{\mathbf{k}} = \gamma_k$; (2) ω_k increases monotonically with k . These assumptions are relevant for most experiments on Bose–Einstein condensation.

Thermalization part of the equation causes the redistribution of the particles in the momentum space and preserves the total number of particles $\sum_{\mathbf{k}} n_{\mathbf{k}}(t)$. Indeed, from (1) it follows

$$\frac{d}{dt} \sum_{\mathbf{k}} n_{\mathbf{k}}(t) = - \sum_{\mathbf{k}} \gamma_{\mathbf{k}} n_{\mathbf{k}}(t) + \sum_{\mathbf{k}} \varkappa_{\mathbf{k}}(t). \quad (2)$$

Regarding the thermalization process, we assume that (1) the thermalization rate is zero between the states separated by the energies over $\hbar\omega_M$, i.e. $\gamma_{\text{therm}}^{\mathbf{k}_1\mathbf{k}_2} = 0$ for $|\omega_{k_1} - \omega_{k_2}| > \omega_M$; (2) the thermalization rate depends only on the difference between the energies of the states such that

$$\gamma_{\text{therm}}^{\mathbf{k}_1\mathbf{k}_2} = \gamma_{\text{therm}}^{k_1 k_2} = \Gamma (1 + n_{\text{th}}(\omega_{k_2} - \omega_{k_1})) \quad \text{for } |\omega_{k_1} - \omega_{k_2}| < \omega_M \text{ and } \omega_{k_1} < \omega_{k_2}, \quad (3)$$

and

$$\gamma_{\text{therm}}^{\mathbf{k}_1\mathbf{k}_2} = \gamma_{\text{therm}}^{k_1 k_2} = \Gamma n_{\text{th}}(\omega_{k_1} - \omega_{k_2}) \quad \text{for } |\omega_{k_1} - \omega_{k_2}| < \omega_M \text{ and } \omega_{k_2} < \omega_{k_1}, \quad (4)$$

* vladislavmipt@gmail.com

† anton.zasedatelev@univie.ac.at

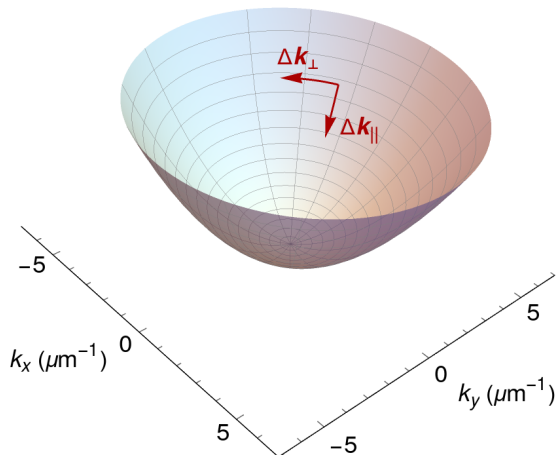


FIG. 1. Energy-momentum relation of the particles. For the illustrative purposes we show a two-dimensional system with the particles having a parabolic dispersion. For the illustrative purposes, we also specify the momentum range from $-7 \mu\text{m}^{-1}$ to $7 \mu\text{m}^{-1}$ which is relevant for the recent experiments [9–12]. Red arrows on the dispersion surface show perpendicular $\Delta\mathbf{k}_\perp$ and parallel $\Delta\mathbf{k}_\parallel$ components of the wave-vector, exchanged within the process of particle thermalization.

where Γ is a constant rate, $n_{\text{th}}(\Delta\omega) = (e^{\hbar\Delta\omega/k_B T} - 1)^{-1}$, T is the temperature of the environment, and k_B is the Boltzmann constant. These assumptions are consistent with the Kubo–Martin–Schwinger relation [8], $\gamma_{\text{therm}}^{\mathbf{k}_1\mathbf{k}_2} = \gamma_{\text{therm}}^{\mathbf{k}_2\mathbf{k}_1} e^{-(\hbar\omega_{\mathbf{k}_1} - \hbar\omega_{\mathbf{k}_2})/k_B T}$.

The momentum \mathbf{k} in Eq. (1) are discrete, and their manifold is determined by the size of the system. We make a transition from the discrete manifold to the continuous distribution of the momentum introducing the linear density of the particles

$$f(k, t) = \sum_{\mathbf{K}} n_{\mathbf{K}}(t) \delta(|\mathbf{K}| - k), \quad (5)$$

where the sum is taken over all the states with the same absolute momentum \mathbf{k} . The introduction of the linear density (5) allows us not only to pass from discrete momenta to a continuous momentum k in Eq. (1), but also exclude thermalization dynamics along the states with perpendicular momenta, as shown in Fig. 1.

One can see that the thermalization rate given by (3)–(4) does not depend on $\Delta\mathbf{k}_\perp$ (see Fig. 1). Thus, using the definition of the linear density (5), we can transform the discrete Maxwell–Boltzmann equation (1) into the

continuous form

$$\begin{aligned} \frac{\partial f(k, t)}{\partial t} = & -\gamma_k f(k, t) + F(k, t) \\ & + \int_0^{+\infty} (\gamma_{\text{therm}}^{kk'} - \gamma_{\text{therm}}^{k'k}) f(k, t) f(k', t) dk' \\ & + \int_0^{+\infty} [\gamma_{\text{therm}}^{kk'} g(k) f(k', t) - \gamma_{\text{therm}}^{k'k} g(k') f(k, t)] dk'. \end{aligned} \quad (6)$$

where $F(k, t) = \sum_{\mathbf{K}} \varkappa_{\mathbf{K}}(t) \delta(|\mathbf{K}| - k)$ is an incoherent pumping and $g(k) = \sum_{\mathbf{K}} \delta(|\mathbf{K}| - k)$ is the density of states determined by the dimensionality of the system. For a one-dimensional system $g(k) = L/2\pi$, where L is the length of the system; for a two-dimensional system $g(k) = Sk/2\pi$, where S is the area of the system; for a three-dimensional system $g(k) = Vk^2/2\pi^2$, where V is the volume of the system.

So far, Eq. (6) is equivalent to Eq. (1) which is the Maxwell–Boltzmann equation. To transform the integral equation (6) into the equation of a differential type, we integrate over the momentum space preserving only the terms up to ω_M^2 (see Appendix A for details). As a result, we obtain the convection–diffusion equation describing the kinetics of Bose gas

$$\frac{\partial f(k, t)}{\partial t} + \frac{\partial J(k, t)}{\partial k} = -\gamma_k f(k, t) + F(k, t) \quad (7)$$

with the flux in momentum space defined by

$$\begin{aligned} J(k, t) = & -\frac{\Gamma\omega_M^2}{2} \frac{g(k)f(k, t)}{v_{\text{gr}}^2(k)} \\ & - \frac{k_B T}{\hbar} \frac{\Gamma\omega_M^2}{2} \frac{g^2(k)}{v_{\text{gr}}^3(k)} \frac{\partial}{\partial k} \left(\frac{f(k, t)}{g(k)} \right) - \frac{\Gamma\omega_M^2}{2} \frac{f^2(k, t)}{v_{\text{gr}}^2(k)}. \end{aligned} \quad (8)$$

The left-hand side of Eq. (7) corresponds to the conservative dynamics with the particle redistribution over momentum space caused by thermalization, while the right-hand side of this equation is the non-conservative part, which describes the loss of particles, $-\gamma_k f(k, t)$, and the supply of particles to the system from some external source, $F(k, t)$. Since $k = |\mathbf{k}|$, the particles cannot pass through $k = 0$ implying the boundary condition for Eq. (7)

$$\lim_{k \rightarrow +0} J(k, t) = 0. \quad (9)$$

The convection–diffusion equation in momentum space (7) with boundary condition (9) and the expression for the flow of the particles in momentum space (8) are the main result of the paper. In what follows, we study the properties of the obtained equation with the main focus on two-dimensional systems with a parabolic dispersion.

III. GENERAL PROPERTIES OF THE CONVECTION-DIFFUSION EQUATION (7)

Similar to the Maxwell-Boltzmann equation (1), the thermalization term, $\partial J(k, t)/\partial k$, in Eq. (7) contains both linear component (the first two terms on the right-hand side of Eq. (8)) and a non-linear component (the last term on the right-hand side of Eq. (8)). However, unlike the Maxwell-Boltzmann equation (1), the equation governing the linear density (7) is local with respect to k , which facilitates both analytical and numerical analysis. Notably, the thermalization property of the Maxwell-Boltzmann equation (1), which ensures conservation of the total number of particles, holds for Eq. (7). Indeed, from Eq. (5) and (7), it follows $\int_0^{+\infty} f(k, t) dk = \sum_{\mathbf{k}} n_{\mathbf{k}}(t)$ and $(\partial/\partial t) \int_0^{+\infty} f(k, t) dk = -\gamma_k \int_0^{+\infty} f(k, t) dk + \int_0^{+\infty} F(k, t) dk$ which is equivalent to Eq. (2).

In the conservative scenario, $\gamma_k = 0$ and $F(k, t) = 0$ in Eq. (7), the stationary linear density of the particles, $f_{\text{St}}(k)$, follows the equation $J = 0$, thus, from Eq. (8) we have

$$\frac{g(k)f_{\text{St}}(k)}{v_{\text{gr}}^2(k)} + \frac{k_B T}{\hbar} \frac{g^2(k)}{v_{\text{gr}}^3(k)} \frac{\partial}{\partial k} \left(\frac{f_{\text{St}}(k)}{g(k)} \right) + \frac{f_{\text{St}}^2(k)}{v_{\text{gr}}^2(k)} = 0 \quad (10)$$

It is easy to see, that the linear density

$$f_{\text{St}}(k) = \frac{g(k)}{e^{(\hbar(\omega_k - \omega_0) - \mu)/k_B T} - 1}, \quad (11)$$

corresponding to the Bose-Einstein distribution, $n_{\mathbf{k}} = (e^{(\hbar(\omega_{\mathbf{k}} - \omega_0) - \mu)/k_B T} - 1)^{-1}$ with the chemical potential μ , is the solution of Eq. (10). Thus, in the conservative scenario, Eq. (7) reproduces Bose-Einstein distribution as the steady-state solution.

IV. 2D BOSE GAS WITH PARABOLIC DISPERSION

For a 2D system with the area S , as it was mentioned above, $g(k) = Sk/2\pi$. The parabolic dispersion implies $\omega_k = \omega_0 + \alpha k^2$, consequently, $v_{\text{gr}}(k) = 2\alpha k$. As a result, from Eq. (7) we obtain

$$\begin{aligned} \frac{\partial f(k, t)}{\partial t} &= -\gamma_k f(k, t) + \frac{v}{2} \frac{\partial}{\partial k} \left(\frac{f(k, t)}{k} \right) + \\ \frac{D}{4} \frac{\partial}{\partial k} \left(\frac{1}{k} \frac{\partial}{\partial k} \left(\frac{f(k, t)}{k} \right) \right) &+ \frac{b}{8\pi} \frac{\partial}{\partial k} \left(\frac{f^2(k, t)}{k^2} \right) + F(k, t), \end{aligned} \quad (12)$$

where we introduced the coefficients

$$D = \frac{k_B T}{\hbar} \frac{S}{8\pi\alpha^3} \Gamma\omega_M^2, \quad (13)$$

$$v = \frac{S}{8\pi\alpha^2} \Gamma\omega_M^2, \quad (14)$$

$$b = \frac{\pi}{\alpha^2} \Gamma\omega_M^2. \quad (15)$$

A very important property of these coefficients is that the ratios between them depend only on the size of the system S , dispersion coefficient α , and the temperature T .

A. Bateman-Burgers equation

While the linear density of particles (5) is quite convenient for theoretical analysis, it appears to be not very practical quantity for experimental observation of two-dimensional systems. Instead, the average density, $\rho(k, t)$, defined by

$$\rho(k, t) = \frac{f(k, t)}{2\pi k} \quad (16)$$

can be easily accessed in standard dispersion imaging measurements, schematically shown in Fig. 2. Specifically, Fig. 2c shows the typical experimental setup to measure particle density in energy and momentum space. Here, the light from the cavity is collected in the confocal configuration, and then projected onto the slit of the spectrometer [11–17]. The lens produces a far-field (Fourier) image in the focal plane (Fig. 2d). The image is then projected on the entrance slit of the spectrometer such that only a narrow region around $k_y = 0$ is coupled in (Fig. 2d). Symmetric projection of the momentum space onto the slit ensures that the total number of particles within the region of interest (yellow square in Fig. 2e) is proportional to the average density (16). By integrating the emission over the frequencies within interval Δk_x around k_x (yellow rectangular in Fig. 2f) one can immediately obtain the average particle density $\rho(|k_x|, t)$ (16). Now, using the resultant equation (12) for the linear density, $f(k, t)$, we can get an equation for the evolution of the average particles density

$$\frac{\partial \rho}{\partial t} = -\gamma_k \rho + v \frac{\partial \rho}{\partial(k^2)} + D \frac{\partial^2 \rho}{\partial(k^2)^2} + b\rho \frac{\partial \rho}{\partial(k^2)} + P \quad (17)$$

where $\rho = \rho(k, t)$ and $P(k, t) = F(k, t)/2\pi k$ is an incoherent pumping term. The general boundary condition Eq. (9) corresponds to the specific boundary condition for the average density of the particles in two-dimensional system with parabolic potential

$$v\rho(0, t) + D \frac{\partial \rho(0, t)}{\partial(k^2)} + \frac{b}{2} \rho^2(0, t) = 0. \quad (18)$$

Eq. (17) is very similar to the well-known Bateman-Burgers equation, which appears in fluid mechanics [6] describing turbulent flows, as well as the formation of shock waves [18]. We identify three major deviations from the standard Bateman-Burgers dynamics, namely: (i) – the dissipation term $\gamma_k \rho$ corresponding to the loss of particles with the rate γ_k ; (ii) – the drift term $v\partial\rho/\partial(k^2)$ with the constant velocity v towards the ground state

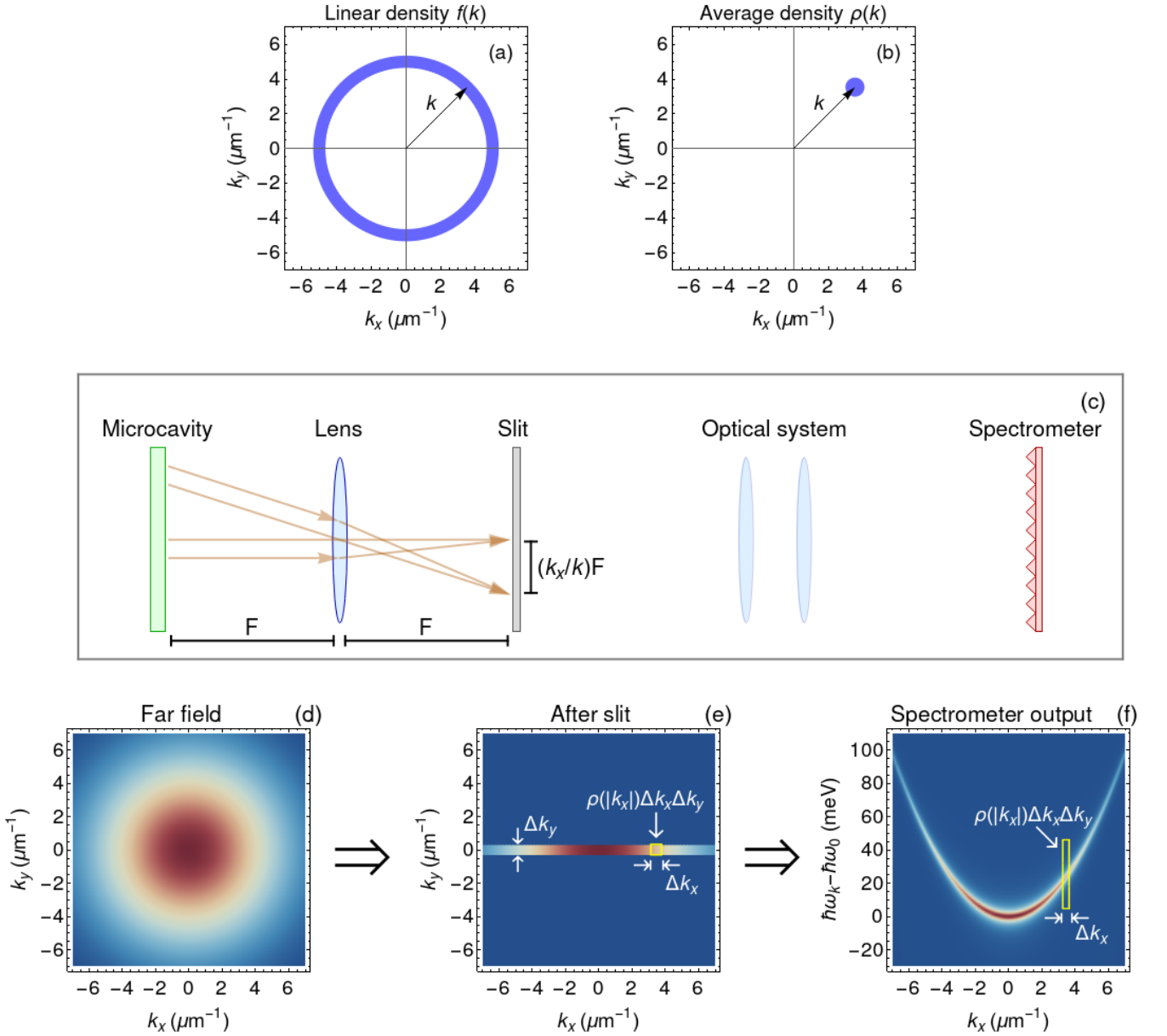


FIG. 2. Schematic of (a) the linear density (5) and (b) the average density (16) for a two-dimensional system. Typical experimental setup to access average particle density (c). The light from the cavity is collected in the confocal configuration resulting in far field (Fourier) image - momentum space (d). The image is then projected to a slit of the spectrometer, $k_y = 0$ as it is shown in (e). Each pixel column at the CCD camera corresponds to frequency and each pixel row corresponds to the in-plane momentum of the emitted light. The illustration of the resultant data is shown in (f). We set the parameters as follows $\hbar\alpha_{\text{cav}} = 2$ (meV $\cdot \mu\text{m}^2$), $\hbar\gamma_k = 5$ (meV) for all the cavity modes which is relevant for the recent experiments [9, 11, 12].

$k = 0$; and (iii) – the semi-boundness of the momentum space ($k > 0$) which leads to the boundary condition (18).

Following, the hydrodynamic analogy we introduce the Reynolds number, Re , by the ratio of the inertia forces (non-linear term $(b/2)\partial\rho^2/\partial(k^2)$) to viscous forces (diffusion term $D\partial^2\rho/\partial(k^2)^2$) [19, 20]

$$Re = \left[\frac{b\rho^2}{4k\Delta k} \right] \cdot \left[\frac{D\rho}{(2k\Delta k)^2} \right]^{-1} = \frac{N}{G_{2D}} \quad (19)$$

where Δk is the characteristic scale of the particles distribution over absolute momentum, $G_{2D} = Sk_B T / 4\pi\hbar\alpha$ is the number of states within the energy region ($\hbar\omega_0$, $\hbar\omega_0 + k_B T$) [21], and $N = \sum_{\mathbf{k}} n_{\mathbf{k}} \approx 2\pi k \Delta k \rho(k)$ is the total number of particles. Large Reynolds number, $Re \gg 1$, corresponds to strong non-linear dynamics, whereas small Reynolds number, $Re \ll 1$, describes the linear regime of the density evolution in the momentum space, comprising the diffusion and drift towards $k = 0$.

When the Reynolds number approaches unity, $Re = 1$, the system undergoes a transition to non-equilibrium Bose–Einstein condensation [21], establishing the critical threshold within the hydrodynamical formalism.

B. Solution of Bateman–Burgers equation

Given that a high-momentum state is initially occupied – created, for example, by an external seed beam injecting particles into the system at k_{seed} – we can directly determine the time t_0 required for the population to reach the ground state using Eq. (17). In the regime below condensation threshold, where $Re < 1$, we have mainly two terms: the drift and the diffusion, which leads to

$$t_0 = \frac{k_{\text{seed}}^4}{2D} \left(\frac{1}{2} + \frac{\hbar\alpha k_{\text{seed}}^2}{2k_B T} + \sqrt{\frac{1}{4} + \frac{\hbar\alpha k_{\text{seed}}^2}{2k_B T}} \right)^{-1} \quad (20)$$

Therefore, in order for particles to reach the ground state, it is necessary that $t_0 < \gamma_{k=0}^{-1}$. When $\hbar\alpha k_{\text{seed}}^2 \lesssim k_B T$, Eq. (20) results in $t_0 \propto T^{-1}$, which is in agreement with experimental observations of thermalization in exciton-polariton systems at room temperature [10].

Upon reaching the ground state, the thermalization dynamics undergoes a significant change. To tackle this problem, we analyze the conservative limit ($\gamma_k = 0$) of Eq. (17), which reduces to the Bateman–Burgers equation with drift term in a semi-bounded space. We obtain the stationary solution for the average particle density (see Appendix B)

$$\rho_{\text{St}}(k) = \frac{S}{4\pi^2} \frac{1}{e^{(\hbar\alpha k^2 - \mu)/k_B T} - 1}, \quad (21)$$

where μ is the chemical potential of the particles. Remarkably, the stationary solution of the Bateman–Burgers dynamics of a quantum fluid of light in 2D leads to the Bose–Einstein distribution with Eq. (17) representing the dynamics of the system in momentum space.

Studying the dynamics of the average particle density $\rho(k, t)$ described by Eq. (17) requires a numerical approach. However, the conservative limit of Eq. (17) (with $\gamma_k = 0$ and $P = 0$) can still be solved analytically. For this case, we derive an exact solution that fulfills the boundary condition (18) (see Appendix C)

$$\rho(k, t) = 2 \frac{D}{b} \frac{\partial}{\partial(k^2)} \ln \left[e^{-vk^2/2D} \int_0^{+\infty} G(k, t, k_1) e^{(vk_1^2/2D)} e^{\int^{k_1^2} \rho(k_2, 0) d(k_2^2)} d(k_1^2) \right] \quad (22)$$

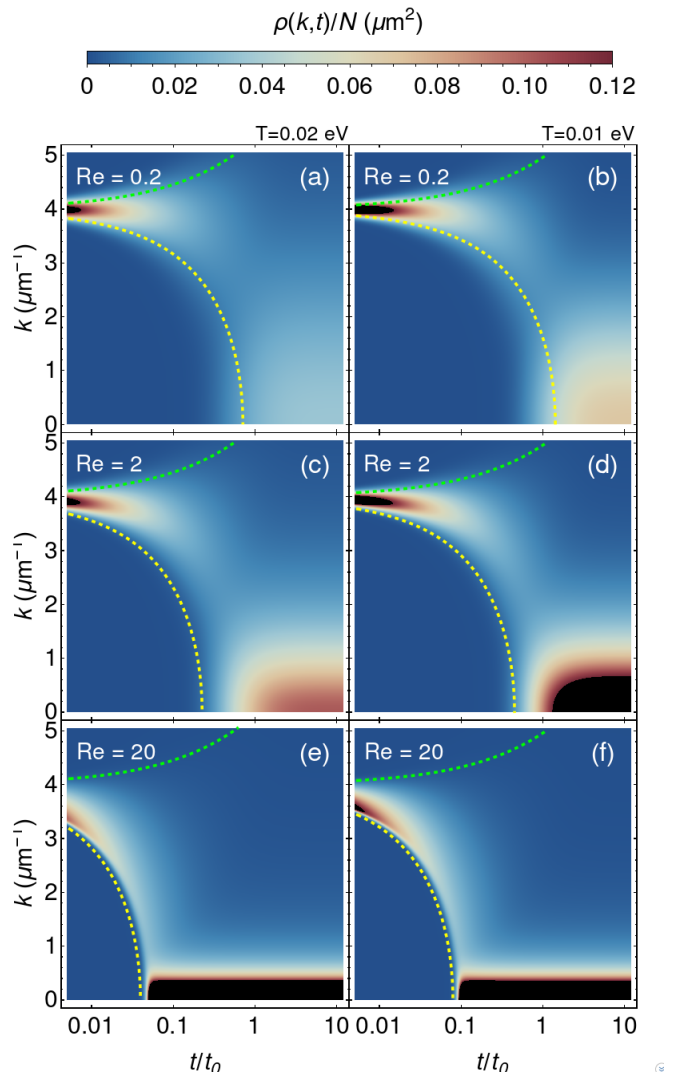


FIG. 3. Conservative dynamics for the average particle density given by Eq. (17) at the different Reynolds numbers (19). The time is normalized to the thermalization time, t_0 , defined by Eq. (20), whereas the average particle density is normalized to the total density, N . The Reynolds numbers are marked on the figures, the corresponding total number of particles is the following: (a) $N = 159$, (b) $N = 80$, (c) $N = 1592$, (d) $N = 798$, (e) $N = 15916$, (f) $N = 7958$. Black regions mark the average densities of the photons surpassing $0.12N \mu\text{m}^2$. The yellow dashed lines mark the leading front, $k_{\text{front}}(t)$, given by Eq. (27) and the green dashed lines back edge, $k_{\text{back}}(t)$, given by Eq. (28). The parameters of the system are $S = 1000 \mu\text{m}^2$, $\hbar\alpha = 2 \text{ meV} \cdot \mu\text{m}^2$, $k_{\text{seed}} = 4 \mu\text{m}^{-1}$, (a, c, e) $k_B T = 20 \text{ meV}$, (b, d, f) $k_B T = 10 \text{ meV}$, in agreement with experimental settings for polariton condensates [10, 12]

where

$$G(k, t, k_1) = \frac{e^{-[(k^2+k_1^2)^2+v^2t^2]/4Dt}}{\sqrt{4\pi Dt}} - \frac{e^{-[(k^2-k_1^2)^2+v^2t^2]/4Dt}}{\sqrt{4\pi Dt}} - \delta(k_1^2) \left[\frac{e^{v^2k^2/4D}}{2} \Phi\left(\frac{k^2+vt}{\sqrt{4Dt}}\right) + \frac{e^{-v^2k^2/4D}}{2} \Phi\left(\frac{k^2-vt}{\sqrt{4Dt}}\right) \right] \quad (23)$$

and $\Phi(\xi)$ is the complementary error function.

We use this result (22) to capture the main features of the thermalization dynamics of quantum fluids of light. Our setup is based on the preoccupied high-momentum states, which can be seeded optically \mathbf{k}_{seed} [9, 22]. Following this setup, we consider an initial condition

$$\rho(k, 0) = Re \cdot \frac{2D}{b} \delta(k^2 - k_{\text{seed}}^2) \quad (24)$$

where Re is the Reynolds number. This initial condition corresponds to $N = 2\pi ReD/b$, consistent with $N = G_{2D} \cdot Re$ obtained in Eq. (19). The exact solution for the average particle density in time and in momentum space given initial conditions (24) can be found as follows

$$\rho(k, t) = \frac{2v}{b} \frac{(e^{-\xi_+^2}/\sqrt{\pi v^2 t/D})(1 + e^{k^2 k_{\text{seed}}^2/Dt}) + \Phi(\xi_+)}{e^{vk^2/D} [2(1 - e^{-Re})^{-1} - \Phi(\xi_-)] - \Phi(\xi_+)} \quad (25)$$

where $\xi_{\pm} = (k^2 \pm (k_{\text{seed}}^2 - vt))/\sqrt{4Dt}$. The steady-state solution ($t \rightarrow +\infty$) for the average particle density reproduces Bose-Einstein distribution (21) with chemical potential $\mu = k_B T \ln(1 - e^{-Re})$.

Figure 3 showcases the thermalization dynamics for quantum fluids of light at different Reynolds numbers, Re . In the conservative scenario, the population thermalizes to the ground state $k = 0$ regardless of the Reynolds number. For small and intermediate Reynolds numbers, $Re \lesssim 1$, (Fig. 3a-b), thermalization is linear (drift and diffusion)

$$\rho(k, t) \approx \frac{N}{2\pi} \frac{e^{-(k^2 - k_{\text{seed}}^2 + vt)^2/4Dt}}{\sqrt{\pi Dt}} \quad (26)$$

and the population reaches the ground state in time t_0 , defined by Eq. (20). For $Re > 1$ thermalization dynamics becomes nonlinear, speeding up the process by t_0/Re approximately. For $Re \gg 1$ and $t \lesssim t_0/Re$ we observe the abrupt change in the average particle density at the leading front (Fig. 3) resembling a shock wave in fluid mechanics [6]. In this case, the momentum of the leading edge of the shock wave, $k_{\text{front}}(t)$, and the tailing edge of the shock wave, $k_{\text{back}}(t)$, are

$$k_{\text{front}}^2(t) = k_{\text{seed}}^2 - \sqrt{\pi ReDt} - \sqrt{2Dt}, \quad (27)$$

$$k_{\text{back}}^2(t) = k_{\text{seed}}^2 + \sqrt{2Dt}, \quad (28)$$

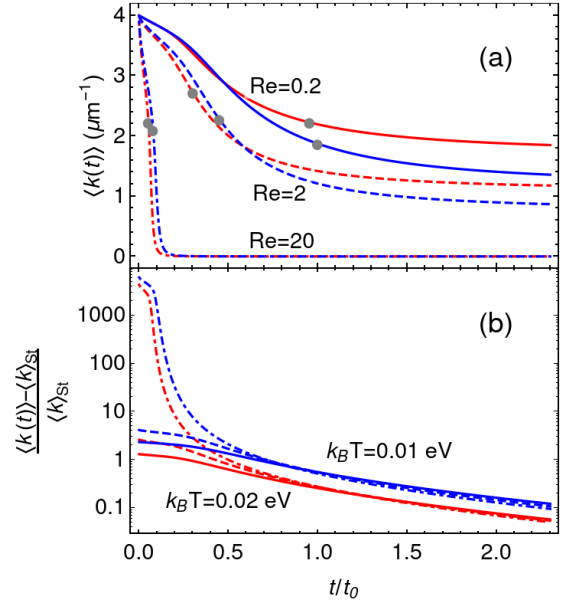


FIG. 4. a - The evolution of $\langle k(t) \rangle$ for different Reynolds numbers: $Re = 0.2$ (solid lines), $Re = 2$ (dashed lines), $Re = 20$ (dot-dashed lines) at different temperature. Red lines correspond to $k_B T = 0.02$ eV and blue lines corresponds to 0.01 eV. Gray dots in (a) mark the time $k_{\text{front}}(t) = 0$. Time t_0 defined by Eq. (20) is different for different temperatures. b - The evolution of the relative deviation of the average momentum, $\langle k(t) \rangle$, from the stationary average momentum, $\langle k \rangle_{\text{st}}$.

Eq. (28) stands for the diffusion of the tailing edge of the shock wave, whereas Eq (27) reveals non-trivial dynamics for the leading edge. First, thermalization in the non-linear regime accelerates by a factor of Re . Second, the leading edge of the shock wave also diffuses, shifting the shock front by $\sqrt{2Dt}$ toward $k = 0$. Both the leading front k_{front} and the back edge k_{back} are shown in Fig. 3e,f. They not only closely follow the leading and tailing edges of the shock wave ($Re \gg 1$) but also describe the kinetics of the Bose gas for lower Reynolds numbers (Fig. 3a-d).

The density inside the shock wave ($Re \gg 1$) has the form $\rho(k, t) \approx B(t) \cdot (k_{\text{back}}(t) - k)$ for $k_{\text{front}}(t) \leq k \leq k_{\text{back}}(t)$ and $\rho = 0$ otherwise with a coefficient $B(t)$ analogous to Ref. [6]. We define $B(t)$ such that the total particle number, N , is conserved in time and obtain the approximate expression for the evolution of the average particle density for $k_{\text{front}}(t) \leq k \leq k_{\text{back}}(t)$

$$\rho(k, t) \approx \frac{3N(k_{\text{back}}(t) - k)}{\pi(k_{\text{back}}(t) - k_{\text{front}}(t))^2(2k_{\text{front}}(t) + k_{\text{back}}(t))} \quad (29)$$

which is valid as long as $k_{\text{front}}(t) > 0$.

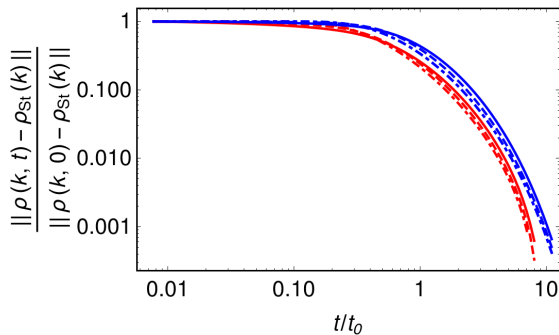


FIG. 5. The evolution of the *distance* (31) in average particle density, $\rho(k, t)$, from its stationary distribution $\rho_{\text{St}}(k)$ plotted for different Reynolds numbers: $Re = 0.2$ (solid lines), $Re = 2$ (dashed lines), $Re = 20$ (dot-dashed lines) at different temperature. Red lines correspond to $k_bT = 0.02$ eV and blue lines corresponds to 0.01 eV. Time t_0 defined by Eq. (20) is different for different temperatures.

C. Dynamics of BEC formation

We analyze the leading front $k_{\text{front}}(t)$ and propose it as a measure of the evolution of the particles density $\rho(k, t)$ up to the point where $k_{\text{front}}(t) = 0$. Once the ground state is reached, this measure becomes ineffective for characterizing $\rho(k, t)$, prompting us to introduce an average absolute momentum of the particles, defined as follows:

$$\langle k(t) \rangle = \frac{\int_0^{+\infty} k \rho(k, t) dk}{\int_0^{+\infty} \rho(k, t) dk}, \quad (30)$$

which retains its physical meaning even when $k_{\text{front}}(t)$ reaches the ground state. In the limit of $t \rightarrow \infty$, the average momentum $\langle k(t) \rangle$ asymptotically reaches $\langle k \rangle_{\text{St}} = \int_0^{+\infty} k \rho_{\text{St}}(k) dk / \int_0^{+\infty} \rho_{\text{St}}(k) dk$, where ρ_{St} is defined by Eq. (21) (Fig. 4a). Similarly to k_{front} the dynamics of the average momentum, $\langle k(t) \rangle$, accelerates with the Reynolds number (Fig. 4a). The evolution of $\langle k(t) \rangle$ exhibits universal evolution after the time t_0 defined by Eq. (20). Indeed, the evolution of relative deviation of the average momentum from the stationary average momentum, $(\langle k(t) \rangle - \langle k \rangle_{\text{St}}) / \langle k \rangle_{\text{St}}$ does not depend on the Reynolds number for a fixed temperature (Fig. 4b).

The universal dynamics of $\langle k(t) \rangle$ suggests a corresponding universal time evolution of $\rho(k, t)$. To demonstrate this, we introduce the *distance* between density $\rho(k, t)$ at time t and stationary density $\rho_{\text{St}}(k)$.

$$\|\rho(k, t) - \rho_{\text{St}}(k)\| = \int_0^{+\infty} |\rho(k, t) - \rho_{\text{St}}(k)| dk. \quad (31)$$

Figure 5 shows that $\|\rho(k, t) - \rho_{\text{St}}(k)\| / \|\rho(k, 0) - \rho_{\text{St}}(k)\|$ is independent of the Reynolds number for a fixed temperature. This is a non-trivial result, considering the dynamics of $\rho(k, t)$ presented in Fig.3. Indeed, Fig.3 clearly

demonstrates a speed-up in thermalization toward the ground state as the Reynolds number increases. However, Fig. 5 reveals that the overall time required for $\rho(k, t)$ to approach the stationary density $\rho_{\text{St}}(k)$ — as defined by the distance (31) — is a universal measure, t_0 , and remains independent of the Reynolds number.

V. CONCLUSION

We study the kinetics of thermalization of quantum fluids of light. We derive the effective local form of the Maxwell–Bloch equation for the linear particle density in momentum space that takes the form of the convection-diffusion equation. This equation describes the kinetics of the Bose gas in momentum space and reproduces the Bose-Einstein distribution as the steady-state solution in the conservative scenario. In a particular case of a two-dimensional system with parabolic potential, the convection-diffusion equation in momentum space for quantum fluids of light resembles the well-known Bateman–Burgers equation which is widely used in fluid mechanics and describes flow propagation, shock waves, and turbulence. The analogy between thermalization dynamics and fluid mechanics enables us to introduce the Reynolds number for the quantum fluid of light. We demonstrate that a Reynolds number of unity corresponds to the condensation threshold in a two-dimensional Bose gas. We obtain an approximate analytical expression describing the dynamics of the average particle density for arbitrary Reynolds numbers. This result applies to the conservative scenario, relevant to experimental platforms based on high- Q optical cavities. For Reynolds numbers greater than unity, we showed that the particles can form an analog of the shock wave in momentum space, resulting in an abrupt change in the average density at the leading front. Additionally, we highlight the universality in the formation of the Bose–Einstein condensate: while the dynamics of the average photon density approaching its stationary distribution depends on temperature, they show little to no dependence on the Reynolds number.

ACKNOWLEDGMENTS

We thank M. Prüfer for fruitful discussions. A.E.S and Sh.V.Yu. thank Russian Science Foundation (project No. 20-72-10057). P.I.V. thanks the Foundation for the Advancement of Theoretical Physics and Mathematics “Basis”. A.V.Z. acknowledges support from the European Union’s Horizon 2020 research and innovation programme under the Marie Skłodowska-Curie grant agreement No 101030987 (LOREN).

Appendix A: Derivation of the convection-diffusion equation in momentum space for quantum fluids of light

We transform the integral equation (6) into a differential type equation (7). The thermalization process is most efficient for close wave-vectors k and k' due to the factor $n_{\text{th}}(\Delta\omega)$ in (3) and (4). Moreover, the difference between the momentum k and k' is limited by the maximal frequency ω_M , which we illustrate in Fig. 6. Thus, we introduce q_1 and q_2 as a solution of the equations $\omega_k - \omega_{k-q_1} = \omega_M$ and $\omega_{k+q_2} - \omega_k = \omega_M$ corresponding to the maximal absolute momentum that can be transferred in the elementary thermalization process

$$q_1 \approx \frac{\omega_M}{v_{\text{gr}}(k)} + \frac{1}{2} \frac{\omega_M^2}{v_{\text{gr}}^3(k)} \frac{\partial v_{\text{gr}}(k)}{\partial k}, \quad (\text{A1})$$

$$q_2 \approx \frac{\omega_M}{v_{\text{gr}}(k)} - \frac{1}{2} \frac{\omega_M^2}{v_{\text{gr}}^3(k)} \frac{\partial v_{\text{gr}}(k)}{\partial k}, \quad (\text{A2})$$

where we denote the group velocity

$$v_{\text{gr}}(k) = \frac{\partial \omega_k}{\partial k}. \quad (\text{A3})$$

Using Eq. (A1)–(A2) we transform the thermalization part of Eq. (6) preserving the terms proportional to ω_M^2

$$\int_0^{+\infty} (\gamma_{\text{therm}}^{kk'} - \gamma_{\text{therm}}^{k'k}) f(k, t) f(k', t) dk' = \Gamma f(k, t) \left[\int_0^{q_2} f(k+q, t) dq - \int_0^{q_1} f(k-q, t) dq \right] \approx \frac{\Gamma \omega_M^2}{2} \frac{\partial}{\partial k} \left(\frac{f^2(k, t)}{v_{\text{gr}}^2(k)} \right) \quad (\text{A4})$$

and similarly

$$\int_0^{+\infty} \left[\gamma_{\text{therm}}^{kk'} g(k) f(k', t) - \gamma_{\text{therm}}^{k'k} g(k') f(k, t) \right] dk' \approx \frac{k_B T}{\hbar} \frac{\Gamma \omega_M^2}{2} \frac{\partial}{\partial k} \left[\frac{g^2(k)}{v_{\text{gr}}^3(k)} \frac{\partial}{\partial k} \left(\frac{f(k, t)}{g(k)} \right) \right] + \frac{\Gamma \omega_M^2}{2} \frac{\partial}{\partial k} \left(\frac{g(k) f(k, t)}{v_{\text{gr}}^2(k)} \right) \quad (\text{A5})$$

The substitution of Eq. (A4)–(A5) into Eq. (6) allow us to obtain the convection–diffusion equation in momentum space for the linear density (7).

Appendix B: Stationary solution of conservative Bateman–Burgers equation with a drag term

In this Section, we obtain the stationary solution (21). The stationary conservative Bateman–Burgers equation with a drag follows from Eq. (17)

$$v \frac{\partial \rho_{\text{St}}(k)}{\partial (k^2)} + D \frac{\partial^2 \rho_{\text{St}}(k)}{\partial (k^2)^2} + b \rho_{\text{St}}(k) \frac{\partial \rho_{\text{St}}(k)}{\partial (k^2)} = 0 \quad (\text{B1})$$

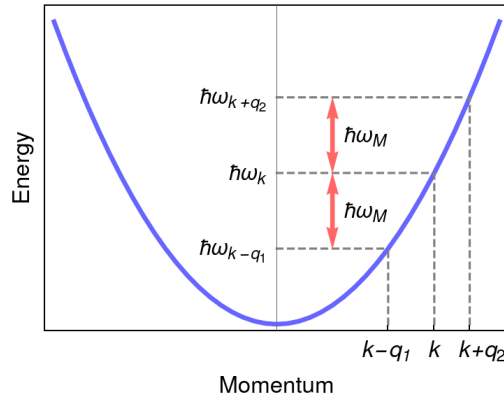


FIG. 6. Schematic representation of the maximum absolute transferred momentum q_1 and q_2 . The equations determining q_1 and q_2 are $\omega_k - \omega_{k-q_1} = \omega_M$ and $\omega_{k+q_2} - \omega_k = \omega_M$. For the illustrative purposes we show a parabolic dispersion.

We integrate this equation over k^2 and obtain

$$v\rho_{\text{St}}(k) + D\frac{\partial\rho_{\text{St}}(k)}{\partial(k^2)} + \frac{b}{2}\rho_{\text{St}}^2(k) = C_1 \quad (\text{B2})$$

The boundary condition (18) implies $C_1 = 0$. Thus, the stationary average density, $\rho_s(k)$, can be obtained from the first-order differential equation

$$v\rho_{\text{St}}(k) + D\frac{\partial\rho_{\text{St}}(k)}{\partial(k^2)} + \frac{b}{2}\rho_{\text{St}}^2(k) = 0. \quad (\text{B3})$$

The general solution of this equation is

$$\rho_{\text{St}}(k) = \frac{2v}{b} \frac{1}{C_2 e^{vk^2/D} - 1}. \quad (\text{B4})$$

where C_2 is some constant. From the definitions of parameters D , v and b , given by Eq. (13)–(15), we obtain

$$\frac{vk^2}{D} = \frac{\hbar\alpha_{\text{cav}}k^2}{k_B T} \quad (\text{B5})$$

and

$$\frac{2v}{b} = \frac{S}{4\pi^2}. \quad (\text{B6})$$

Thus, substitution $C_2 = e^{-\mu/k_B T}$ leads us to Eq. (21).

Appendix C: Exact solution of conservative Bateman–Burgers equation with a drift term

In this Appendix we obtain an analytical solution for Eq. (17) with boundary condition (18).

We use the Cole–Hopf transformation

$$\rho(k, t) = 2\frac{D}{b} \frac{\partial \ln \varphi(k, t)}{\partial(k^2)} \quad (\text{C1})$$

and obtain a diffusion equation with drift for $\varphi(k, t)$

$$\frac{\partial \varphi(k, t)}{\partial t} = v \frac{\partial \varphi(k, t)}{\partial(k^2)} + D \frac{\partial^2 \varphi(k, t)}{\partial(k^2)^2} \quad (\text{C2})$$

with the boundary condition

$$v \frac{\partial \varphi(0, t)}{\partial(k^2)} + D \frac{\partial^2 \varphi(0, t)}{\partial(k^2)^2} = 0. \quad (\text{C3})$$

Following [23] we use another transformation

$$\varphi(k, t) = e^{-vk^2/2D} \psi(k, t) \quad (\text{C4})$$

we obtain a Schrodinger type equation

$$\frac{1}{D} \frac{\partial \psi(k, t)}{\partial t} = \frac{\partial^2 \psi(k, t)}{\partial(k^2)^2} - \left(\frac{v}{2D}\right)^2 \psi(k, t) \quad (\text{C5})$$

with the boundary condition

$$\frac{\partial^2 \psi(0, t)}{\partial(k^2)^2} - \left(\frac{v}{2D}\right)^2 \psi(0, t) = 0 \quad (\text{C6})$$

Our goal is to find propagator $G(k, t, k_1)$ such that we could obtain the solution $\psi(k, t)$ for any initial condition $\psi(k, 0)$

$$\psi(k, t) = \int_0^{+\infty} G(k, t, k_1) \psi(k_1, 0) dk_1. \quad (\text{C7})$$

Such a propagator should at least fulfill four following conditions

$$\frac{1}{D} \frac{\partial G(k, t, k_1)}{\partial t} = \frac{\partial^2 G(k, t, k_1)}{\partial (k^2)^2} - \left(\frac{v}{2D}\right)^2 G(k, t, k_1) \text{ for } k_1 > 0, \quad (\text{C8})$$

$$\frac{\partial^2 G(0, t, k_1)}{\partial (k^2)^2} - \left(\frac{v}{2D}\right)^2 G(0, t, k_1) = 0 \text{ for } k_1 > 0, \quad (\text{C9})$$

$$G(k, 0, k_1) = \delta(k^2 - k_1^2) \text{ for } k_1 > 0 \text{ and } k > 0. \quad (\text{C10})$$

$$G(k, t, k_1) \text{ is limited for } k \rightarrow +\infty \quad (\text{C11})$$

Propagator $G(k, t, k_1)$ allows us to find $\rho(k, t)$ from the initial condition $\rho(k, 0)$ according to Eq. (22).

To find the propagator $G(k, t, k_1)$ we determine the eigenfunction of the Eq. (C5) with the boundary condition Eq. (C6)

$$\psi_\omega(k, t) = \sqrt{\frac{v}{\pi D}} e^{-(v/2D)^2(1+\omega^2)Dt} \sin\left(\frac{v\omega k^2}{2D}\right), \quad (\text{C12})$$

$$\psi_{\text{st}}(k, t) = \sqrt{\frac{v}{\pi D}} e^{-vk^2/2D}. \quad (\text{C13})$$

One can see, that functions $\psi_\omega(k, t)$ and $\psi_{\text{st}}(k, t)$ are not orthogonal. This is because the operator in the right-hand side of Eq. (C5) with the boundary condition (C6) is not Hermitian. Therefore, we cannot directly use the method described in [23]. To overcome the non-orthogonality of $\psi_\omega(k, t)$ and $\psi_{\text{st}}(k, t)$ we introduce a new set of functions

$$\bar{\psi}_\omega(k, t) = \sqrt{\frac{v}{\pi D}} \left[e^{-(v/2D)^2(1+\omega^2)Dt} \sin\left(\frac{v\omega k^2}{2D}\right) - 2\frac{\omega}{1+\omega^2} e^{-vk^2/2D} \right], \quad (\text{C14})$$

that are orthogonal to $\psi_{\text{st}}(k, t)$.

We try to use the standard method [23] to find the propagator $G(k, t, k_1)$

$$G(k, t, k_1) = \psi_{\text{st}}(k, t) \psi_{\text{st}}(k_1, 0) + \int_0^{+\infty} \bar{\psi}_\omega(k, t) \bar{\psi}_\omega(k_1, 0) d\omega \quad (\text{C15})$$

and obtain

$$G(k, t, k_1) = \frac{e^{-(k^2-k_1^2)^2/4Dt} e^{-v^2t/4D}}{\sqrt{4\pi Dt}} - \frac{e^{-(k^2+k_1^2)^2/4Dt} e^{-v^2t/4D}}{\sqrt{4\pi Dt}} + \frac{v}{D} e^{-vk_1^2/2D} e^{-vk^2/2D} + \frac{v}{D} e^{-vk_1^2/2D} \left\{ \text{sh}\left(\frac{vk^2}{2D}\right) - \frac{1}{2} \left[e^{vk^2/2D} \text{erf}\left(\frac{vt+k^2}{\sqrt{4Dt}}\right) - e^{-vk^2/2D} \text{erf}\left(\frac{vt-k^2}{\sqrt{4Dt}}\right) \right] \right\} \quad (\text{C16})$$

This function fulfills the conditions (C8)–(C11), but gives a wrong stationary solution for ρ .

We note that the first two terms of Eq. (C16) fulfill the condition (C15). Also, the first two terms and the last two terms in the right-hand side of Eq. (C16) fulfill the conditions (C8) and (C9) independently. Moreover, if we change the function $(v/D)e^{-vk_1^2/2D}$ to any other function $F(k_1)$ in the last two terms of the right-hand side of Eq. (C16) the resultant propagator still fulfills the condition (C15). To obtain the correct propagator $G(k, t, k_1)$ that preserves the total number of particles, we should replace $(v/D)e^{-vk_1^2/2D}$ in the last two terms of (C16) by $-\delta(k_1^2)$. As a result, we obtain the propagator (23).

[1] I. Carusotto and C. Ciuti, Quantum fluids of light, Reviews of Modern Physics **85**, 299 (2013).

[2] P. Kirton and J. Keeling, Nonequilibrium model of pho-

- ton condensation, *Physical review letters* **111**, 100404 (2013).
- [3] P. Kirton and J. Keeling, Thermalization and breakdown of thermalization in photon condensates, *Physical Review A* **91**, 033826 (2015).
- [4] J. Schmitt, T. Damm, D. Dung, F. Vewinger, J. Klaers, and M. Weitz, Thermalization kinetics of light: From laser dynamics to equilibrium condensation of photons, *Physical Review A* **92**, 011602 (2015).
- [5] G. B. Whitham, *Linear and nonlinear waves* (John Wiley & Sons, 2011).
- [6] P. Orlandi, *Fluid flow phenomena: a numerical toolkit*, Vol. 55 (Springer Science & Business Media, 2000).
- [7] H. Deng, H. Haug, and Y. Yamamoto, Exciton-polariton bose-einstein condensation, *Reviews of Modern Physics* **82**, 1489 (2010).
- [8] R. Kubo, Statistical-mechanical theory of irreversible processes. i. general theory and simple applications to magnetic and conduction problems, *Journal of the Physical Society of Japan* **12**, 570 (1957).
- [9] D. A. Sannikov, A. V. Baranikov, A. D. Putintsev, M. Misko, A. V. Zasedatelev, U. Scherf, and P. G. Lagoudakis, Room temperature, cascadable, all-optical polariton universal gates, *Nature communications* **15**, 5362 (2024).
- [10] J. D. Plumhof, T. Stöferle, L. Mai, U. Scherf, and R. F. Mahrt, Room-temperature bose-einstein condensation of cavity exciton-polaritons in a polymer, *Nature materials* **13**, 247 (2014).
- [11] A. V. Zasedatelev, A. V. Baranikov, D. Urbonas, F. Scafrimuto, U. Scherf, T. Stöferle, R. F. Mahrt, and P. G. Lagoudakis, A room-temperature organic polariton transistor, *Nature Photonics* **13**, 378 (2019).
- [12] A. V. Zasedatelev, A. V. Baranikov, D. Sannikov, D. Urbonas, F. Scafrimuto, V. Y. Shishkov, E. S. Andrianov, Y. E. Lozovik, U. Scherf, T. Stöferle, *et al.*, Single-photon nonlinearity at room temperature, *Nature* **597**, 493 (2021).
- [13] Z. Jiang, A. Ren, Y. Yan, J. Yao, and Y. S. Zhao, Exciton-polaritons and their bose-einstein condensates in organic semiconductor microcavities, *Advanced Materials* **34**, 2106095 (2022).
- [14] J. Kasprzak, M. Richard, S. Kundermann, A. Baas, P. Jeambrun, J. M. J. Keeling, F. Marchetti, M. Szymańska, R. André, J. Staehli, *et al.*, Bose-einstein condensation of exciton polaritons, *Nature* **443**, 409 (2006).
- [15] W. H. Nitsche, N. Y. Kim, G. Roumpos, C. Schneider, S. Höfling, A. Forchel, and Y. Yamamoto, Spatial correlation of two-dimensional bosonic multimode condensates, *Physical Review A* **93**, 053622 (2016).
- [16] A. I. Väkeväinen, A. J. Moilanen, M. Nečada, T. K. Hakala, K. S. Daskalakis, and P. Törmä, Sub-picosecond thermalization dynamics in condensation of strongly coupled lattice plasmons, *Nature communications* **11**, 3139 (2020).
- [17] J. Tang, J. Zhang, Y. Lv, H. Wang, F. F. Xu, C. Zhang, L. Sun, J. Yao, and Y. S. Zhao, Room temperature exciton-polariton bose-einstein condensation in organic single-crystal microribbon cavities, *Nature Communications* **12**, 3265 (2021).
- [18] J. M. Burgers, A mathematical model illustrating the theory of turbulence, *Advances in applied mechanics* **1**, 171 (1948).
- [19] J. Anderson, *EBOOK: Fundamentals of Aerodynamics (SI units)* (McGraw hill, 2011).
- [20] E. Rathakrishnan, *Theoretical aerodynamics* (John Wiley & Sons, 2013).
- [21] V. Y. Shishkov, E. Andrianov, and Y. E. Lozovik, Analytical framework for non-equilibrium phase transition to bose-einstein condensate, *Quantum* **6**, 719 (2022).
- [22] Y. Yoon, J. Deschamps, M. Steger, K. W. West, L. N. Pfeiffer, D. W. Snoke, and K. A. Nelson, Enhanced thermalization of exciton-polaritons in optically generated potentials, arXiv preprint arXiv:2209.13703 <https://doi.org/10.48550/arXiv.2209.13703> (2022).
- [23] H. Risken and H. Risken, *Fokker-planck equation* (Springer, 1996).